AD-A102 136 FOREIGN TECHNOLOGY DIV WRIGHT-PATTERSON AFB OH F/G 20/4
ACTA MECHANICA SINICA (SELECTED ARTICLES),(U)
JUN 81 L JIANBANG, X SHENGJIE, G BENYU
UNCLASSIFIED FTD-ID(RS)T-0412-81 NL

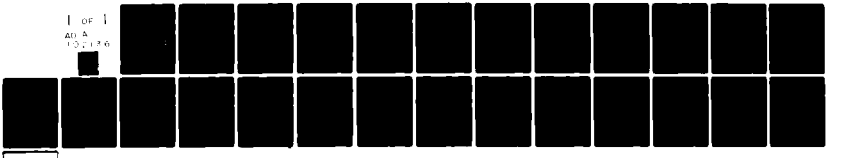

END
DATE FILMED
8-81
DTIC

FTD-ID(RS)T-0412-81

FOREIGN TECHNOLOGY DIVISION

ACTA MECHANICA SINICA

(Selected Articles)

Approved for public release;
distribution unlimited.

FTD-ID(RS)T-0412-81

EDITED TRANSLATION

FTD-ID(RS)T-0412-81   30 Jun[redacted]81

MICROFICHE NR: FTD-C-81-000595

ACTA MECHANICA SINICA (Selected Articles)

~~English pages: 23~~

[redacted] Acta Mechanica Sinica [redacted] 2, [redacted]
[redacted] 147-157

Country of origin: China
Translated by: SCITRAN
F33657-78-D-0619
Requester: FTD/TQTA
Approved for public release; distribution unlimited.

Accession For	
NTIS GRA&I	☒
DTIC TAB	☐
Unannounced	☐
Justification	
By	
Distribution/	
Availability Codes	
Dist	Avail and/or Special
A	

PREPARED BY:

TRANSLATION DIVISION
FOREIGN TECHNOLOGY DIVISION
WP-AFB, OHIO.

141600

TABLE OF CONTENTS

EXPERIMENTAL TECHNIQUE AND EXPERIMENTAL METHOD

PARALLEL CRYSTAL LASER POSITION SHIFT INTEROMETER AND ITS APPLICATION IN FLOW FIELD MEASUREMENT

Liu Jianbang, Xia Shengjie Institute of Mechanics, Academia Sinica

Abstract: The principle of the instrument is to obtain an interference pattern by reflecting from the front and rear surfaces of a parallel crystal laser beam (after beam expansion) after passing it through the system to be measured. The instrument has good vibration-preventive property, and can be used conveniently to measure flow fields with relatively large lateral and longitudinal dimensions. The instrument has high light source intensity and simple structure, and may be easily calibrated and used. It has a good prospect of being widely used in flow field measurement, especially in the measurement of supersonic flow field.

I. Forward

An interferometer is an effective flow field measuring instrument. The commonly used Mach-Zehnder interferometer (abbreviated M-C interferometer) is less tolerant of vibrations, has smaller field of view and depth of measurement. Its light source has lower intensity and hence requires more stringent demand on the measuring environment with more limitations on the lateral and longitudinal ranges of the flow field being measured. It is also difficult to make continuous recording of high speed flow processes. The reasons for these shortcomings are: 1) There are 4 optical elements other than

the light source and the recording element that are involved in the interference process. This creates 3 problems: during exposure there cannot be any relative shifting of positions of the 4 optical elements comparable to a wave-length (this is a major shortcoming of interferometers in general). The method to overcome this problem is to use vibration-free base which tends to make the instrument bulky and heavy, inconvenient both to manufacturing and to utilization; precise calibration of the relative positions of the optical elements is necessary. The more elements there are, the more complicated becomes the calibration process and the more stringent is the demand on the design and construction of the calibration mechanism; optical elements require precision optical work. The more elements there are, the larger will be the quantity of optical work. This is even more so for making an interferometer with a large field of view. 2) Before the advent of the laser, light source intensity for interferometers is low with inferior quality of interference, not suitable for the need of high speed photography as well as imposing limitation on the longitudinal range of the measured flow field.

In this paper we investigage a parallel crystal laser position shift interferometer (abbreviated as parallel crystal interferometer). Its principal feature is that only one single optical element is used to produce the interferogram, namely the front and rear surfaces of a crystal beside the light source and the recording element. Another feature is that a laser is used as the light source. Our work showed that the parallel crystal interferometer has overcome in a great measure the shortcomings of the M-C interferometer mentioned above, and has the prospect to become an interferometer with high utilization value, which may become widely used in flow field measurement.

For the general theory and application of phase shift interferometers may be found in reference [1]. A parallel crystal was used as the basic element of a phase shift interferometer in references [2] and [3] but the method in [2] produced interference fringes with relatively low contrast while reference [3] merely quoted the results of [2]. In this paper we analysed the principle of a parallel crystal interferometer, explained its advantages and disadvantages and their causes, quantitatively analysed the formation of the interference fringes and cited our experimental results.

II. Basic Principles

1. General discussion.

As shown in Figure 1, a laser beam with good directionality and coherence is expanded into a plane wave with a larger cross-section and even better directionality after passing through a beam expander. After travelling through the system

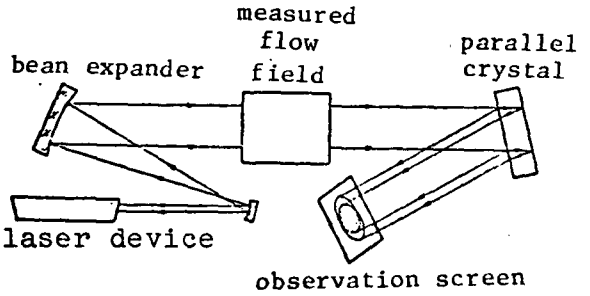

Figure 1. Principle of a parallel crystal interferometer

being measured, it is duly reflected from the front and rear surfaces of a parallel crystal to form two beams with a slight shift in position, the overlapping portion of which now interfere and produce interference fringes on the observation screen. If the measured field flow is ideally uniform, then an ideal

plane wave through it will remain an ideal plane wave. We shall prove below that an ideal plane wave will produce an interference pattern with equi-distant parallel lines after reflecting from the front and rear surfaces of a parallel crystal. Therefore, from the deviation of the interferogram of the measured flow field from a diagram of equi-distant parallel lines, we can make direct qualitative judgment on the density distribution of the measured flow field as well as obtain quantitative conclusions from computation.

2. Theoretical analysis of the interferogram

We assume that the light beam propagates along the z axis in a Cartesian coordinate system xyz. (Figure 2). ϕ_a (x,y) is the phase distribution function in the cross-section area A. The 2 beams reflected from the parallel crystal deviates by an amount Δx along x axis. Δx is called the distance of position shift, and x axis the axis of position shift. The phase distribution functions of the 2 beams on cross-section B are respectively $\phi_{BF}(x,y)$ and $\phi_{BR}(x,y)$. The subscripts "F" and "R" indicate whether the reflection is from the Front or the Rear surface. After reflection, the coordinate system propagates along the reflected beam from the front surface. Hence

$$\phi_{BR}(x, y) = \phi_A(x, y), \quad \phi_{BR}(x,y) = \phi_{BR}(x + \Delta x, y) + a + bx \qquad (1)$$

where a + bx is the phase change due to reflection from the rear surface. It is not difficult to find the constants a and b from the crystal structure, its position and properties of its material. b's value obviously is directly proportional to the angle between the front and rear surfaces of the parallel crystal (i.e. its wedge angle). On cross-section B, ϕ_{BF} (x,y) and $\phi_{BR}(x,y)$ has a phase difference

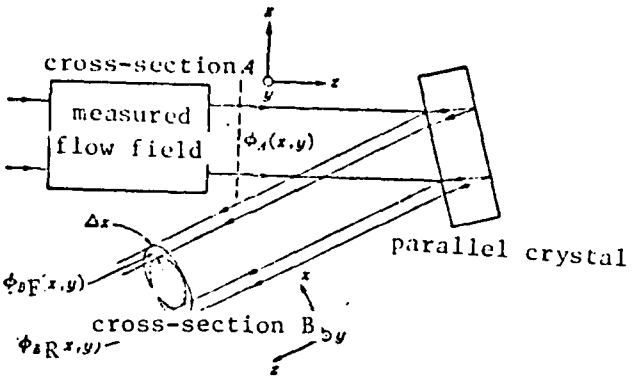

Figure 2

$$\begin{aligned}\Phi_B(x, y) &\equiv \phi_{BL}(x, y) - \phi_{BR}(x, y) \\ &= \phi_{BR}(x + \Delta x, y) + a + bx - \phi_{BR}(x, y) \\ \Delta\phi_A(x, y) &\equiv \phi_A(x + \Delta x, y) - \phi_A(x, y)\end{aligned} \tag{2}$$

By definition
then $$\Phi_B(x, y) = \Delta\phi_A(x, y) + a + bx \tag{3}$$

The surface with equal phase for an ideal uniform flow field is the xy plane, therefore $\phi_A(x,y)\,|_{\text{theory}} = 0$ and hence

$$\Phi_B(x, y)|_R = a + bx \tag{4}$$

$$\Delta\phi_A(x, y) = \Phi_B(x, y) - \Phi_B(x, y)| \tag{5}$$

Now we shall find the phase difference $\phi_A(x_N, y) - \phi_A(x_0, y)$, of 2 points (x_o, y) and (x_N, y) in cross-section A where the difference between x_N and x_o is an integral multiple of the position shift distance, namely $x_N - x_0 = N\Delta x,\ N = 1, 2, \ldots$. We first divide the line segment $x_N - x_o$ into N equal parts, the coordinates of the individual points of division being x_n, n = 0, 1, 2, ..., N. (Figure 3). From equations (2) and (5) we can find

$$\phi_A(x_N, y) - \phi_A(x_0, y) = \sum_{n=0}^{N-1} [\Phi_B(x_n, y) - \Phi_B(x_n, y)|_R] \tag{6}$$

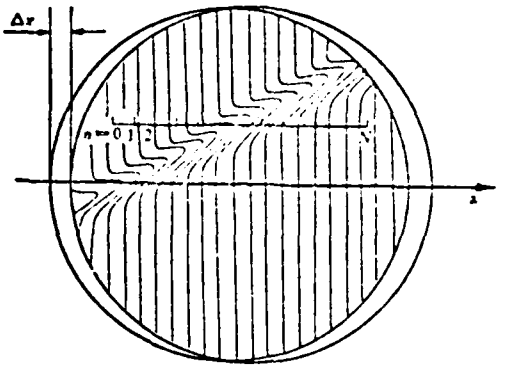

Figure 3

We shall now discuss the above results as follows: 1.) equation (4) shows that for an ideal uniform flow field the phase difference of the 2 beams reflected from the front and rear surfaces of the parallel crystal is directly proportional to x. Therefore, the interferogram of an ideal uniform flow field is a set of equi-distant parallel straight lines normal to the position shift axis, the distance being $2\pi/b$. From this we know that the distance between the parallel lines must be inversely proportional to the wedge angle of the parallel crystal. The deviation of the interferogram of the realistic flow field from that of the ideal uniform flow field is due to the non-uniformity of the density of the medium in the corresponding region. From this we can determine the density distribution of the measured flow field without too much difficulty.

2) From equation (6) we can quantitatively determine the difference in the average density along two straight lines parallel to the optical axis in the measured flow field:

$$\bar{\rho}(x_N, y) - \bar{\rho}(x_0, y) = \frac{1}{l}\int_0^l [\rho(x_N, y, z) - \rho(x_0, y, z)]dz$$

The projections of these two straight lines on the observation screen have coordinates (x_N,y) and (x_o,y) while the two end surfaces of the measured flow field are assumed to be the z=0

and z=1 planes. The process is as follows: Choose the coordinates of the projections of the observation screen of the 2 straight lines to be measured to be (x_N,y) and (x_o,y). They should satisfy $x_n-x_o=N\Delta x$, N=1,2.... Rotate the crystal about its central axis so that the position shift axis is parallel to the line connecting the 2 points. After the interferogram is photographed, read off from it the value of $\phi_B(x_n,y)$ for n=0,1,...,N-1, using (x_o,y) as point 0. Then measure the distance between the interference fringes in the vicinity of (x_o,y) and find the value of b in the equation (4). With (x_o,y) still as the zero point, find the value of $\phi_B(x_n,y)$ ideal at n=0,1,···,N-1 from equation (4), then from equation 6 we can find the phase difference between the points (x_N,y) and (x_o,y) on cross-section A. Finally find

$$\bar{\rho}(x_N, y) - \bar{\rho}(x_0, y) = \frac{\lambda}{2\pi lK}[\phi_A(x_N, y) - \phi_A(x_0, y)] \tag{7}$$

where λ is the wave-length and K is the Glaston-Derr constant.(4)

3) Equation (3) shows that the phase difference $\phi_B(x,y)$ of 2 light rays incident on one point on the observation screen is the sum of the phase difference $\Delta\phi_A(x,y)$ of the corresponding 2 points on the output cross-section of the measured flow field (their distance is equal to the distance of position shift Δx) and the phase difference a + bx of the 2 light rays after being reflected from the front and rear surfaces of the parallel crystal. The value of $\overset{\Delta}{\phi}_A(x,y)$ for various measured flow fields along the direction of the optical axis with different average densities and lengths does not change very much because the light ray in the region of the measured flow field has not yet been split into 2 beams. Magnitudewise, $(\lambda/2\pi)\Delta\phi_A(x, y)$ is generally of the order of the wave length, and $(\lambda/2\pi)(a + bx)$ is generally of the order of centimeters, i.e. $(a + bx) \gg \Delta\phi_A(x, y)$. Hence in the parallel crystal inter-

ferometer, the value of the optical path difference of the 2 interfering beams is primarily determined by $(\lambda/2\pi)(a + bx)$ namely by the characteristics of the parallel crystal and its value is of the order of several centimeters. Therefore the parallel crystal interferometer does not require the use of the compensator that is commonly used in M-C interferometers, which is calibrated according to the length of the optical path of the measured flow field. Also the requirement on the coherent length of the laser light source is not very stringent.

3. Advantages and disadvantages

1. The principle optical elements that produce the interference effect in the M-C interferometer are the 2 beam splitters and the 2 reflecting mirrors. Any small change in the relative positions of these 4 elements will affect the optical path difference of the 2 interfering beams; the parallel crystal interferometer uses only 1 optical element to produce interference. Even under strong vibrations, the stability of the relative position of the front and rear surfaces of the parallel crystal remains to be unquestionable. This is the reason why the parallel interferometer has the capability to withstand strong vibrations.

2. The measured flow field is placed between the parallel beam expander and the crystal where the beam has not yet been split, therefore the relative vibration of the beam splitter, the measured system and the crystal has no effect on the optical path length difference between the 2 interfering beams; as shown on the observation screen, the field of view of the interferogram may have considerable vibrations but the interference fringes themselves remain stable. In practice, the beam splitter, the measured system and the parallel crystal may be mounted on three independent stands which require no special set up to eliminate vibrations. This greatly simplifies the

experimental set up and facilitates the measurement of flow field with relatively large longitudinal (along optical path direction) dimension (it is entirely feasible to measure flow field several meters in length). In addition, the 4 optical elements that produce the interference effect in the M-C interferometer subtend an angle of 45° with the optical axis so that their diameters should be $\sqrt{2}$ times that of the light beam. Two compensator windows with diameters slightly larger than the beam diameter are also required. In the parallel crystal interferometer there is only one optical element to produce the interference effect with its angle subtended with the incident beam nearly perpendicular and hence its diameter needs only be slightly larger than that of the beam. There is no need for a compensator in the parallel crystal interferometer, thereby lowering considerably the demand for optical work and moulding for optical element vis a vis the M-C interferometer.

3. With the laser as the light source, the intensity is much higher, making it possible to make continuous recording of high speed processes with high speed cameras.

4. Simplicity in structure and convenience in calibration and utilization are reflected in fewer optical elements, simple supporting stands, relaxed requirement on the coherent length of the laser light source, the elimination of compensators, the lack of necessity to make precise calibrations on the relative positions of different optical elements, the directness of the observed results, etc.

5. The disadvantage is that in determining the average density difference of 2 straight lines in the flow field quantitatively, it is necessary to add several observed results together, making the procedure more complicated than that for

the M-C interferometer; for any non-transparent object in the flow field, there will be "double shadow" around the edge of the object on the observation screen. Although this effect may be reduced by shortening the position shift, yet in general it cannot be completely eliminated. We must point out that there is no double shadow in the interference fringes so that the effect of the double shadow generally will not affect the result of measurement. It will only give some uncomfortable feeling to the observation.

III. Experimental set up and experimental results

The parallel crystal interferometer may be subdivided into 3 parts: the parallel light source, the parallel crystal and the recording device. The parallel light source consists of the laser and the parallel beam expander. An ordinary single mode continuous output or pulsed output laser tube may be used for the laser. For the parallel beam expander, we may use either the transmitting or the reflecting type. Its effect is to expand the beam diameter to the desired size and to reduce the angle of divergence to obtain a better plane wave. The parallel beam expander should be focused to infinity. The diameter of the beam incident on the object lens should be slightly larger than the diameter of the lens so that only the central portion of the beam is transmitted in order to warrant a more uniform intensity. The position of the laser and the beam expander should be suitably arranged so that the hot air flow produced by the laser tube will not affect the quality of the beam. The laser and the beam expander should be mounted on the same base support to reduce the movement of the field of view induced by vibration. We used as light source a single mode continuous output HeNe laser with a power rating of 1 mW. A reflecting optical path beam expander was used with an eyepiece of focal length 15 mm, and an objective of focal length

1 m and diameter 120 mm. The output beam was good with uniform intensity. The structure of the beam expander and its support is shown in photo 1 on picture page 1.

The front and rear surfaces of the parallel crystal should be good quality optical surfaces without any coating. The wedge angle should be between a few seconds and a few ten's of seconds. There is no strict requirement except to produce an interference pattern with suitable distance between the fringes. We used a wedge angle of 6". The first and second reflected light from the front and rear surfaces of the un-coated crystal had nearly equal intensity while that of the third and higher reflection are rather weak, producing an interferogram with good contrast. There was practically no effect on the interferogram from the 3rd and higher reflected light. For example, if the parallel crystal is made of K_9 glass with an index of refraction of 0.042, then the ratio of the incident light intensity to the first few reflected and transmitted light intensity are shown in Figure 4. It is easy to show that in the interferogram of the first and second reflected light the

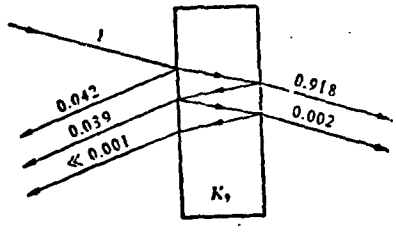

Figure 4. Intensity ratio of incident light and the first few reflected and transmitted light for a K_9 glass crystal.

intensity of the darkest spot is only 0.006 times that of the brightest spot. Hence the bright-dark contrast of the interferogram is close to ideal. The transmitted part is about 92%, which may be used for other measurements.

The recording may be done by direct observation on the screen or by still camera or high speed movie camera. The observation screen is a flat white diffuse reflecting surface. A piece of ground glass may also be used. When the fringes are too crowded, an enlarging device may be used in front of the screen. If a still camera or a high speed movie camera is used, it may be mounted without the lens in place of the screen to record the interferogram directly on the film.

The three parts mentioned above were mounted separately on 3 independent stands (photo 1 picture, page 3). The stands have no special vibration-isolating device.

After the proper installation of the apparatus, an interferogram will appear on the screen. Since now the observed region contains uniform density air, the interferogram should consist of equi-distant parallel straight lines perpendicular to the position shift axis. From this we can examine the quality of the beam expander and of the crystal. According to experimental need, we may rotate the crystal about the central axis to obtain the required fringe direction and then about the y axis to calibrated the distance of position shift. Finally the recording device is to be calibrated. Except the recording device, the whole calibration procedure may be accomplished in a few minutes.

The experimental results are as follows: Photo 2, picture page 5 shows the interferogram of uniform density air in the region of measurement. It approaches very closely the equi-distant parallel straight lines normal to the axis of position shift as calculated from equation (4). Photo 3, picture page 6 is one of the interferograms oblique laser beam recorded continuously with a high speed movie camera for a super-sonic experiment under strong vibration. The precision of this type

of measurement depends on the method to measure the distance between the fringes. Photo 4 in picture page 11 is the interferogram of the warm air flow field near a human hand. From the manifest curvature of the fringes at the palm we can see that the parallel crystal interferometer is relatively sensitive.

Because of the position shift of the two reflected beams due to the thickness of the crystal and the incident angle, double shadow appears in the interferogram. The thicker is the crystal and the larger the angle of incidence, the more separation is there in the double shadow. To overcome this disadvantage, we shall reduce the thickness of the crystal so that the two shadows will approach each other and overlap. For this purpose, we adopted an interference element (Figure 5) consisting of a prism and a plane mirrow. The prism is in contact with the mirror with a thin layer of air between them. The parallel beam is incident on the prism after traversing the measured system at almost right angle and is reflected at the two surfaces in front and at rear of the air gap and then emerges from the other surface of the prism. Interference is produced due to the phase difference of the light reflected by the two surfaces. This basically is a multiple interference and is different from the parallel crystal interferometer discussed above. Since the air gap is very thin, the position shift of the reflected beams from the two surfaces is also very small. If the air gap thickness is of the order of a micrometer, then the position shift is also of the order of a micrometer and the fuzziness of the profile of the model in the interferometer will also be of the order of a micro-meter. According to photographic theory, a picture is sharp when the diameter of the fuzzy element is less than 0.1 -- 0.05 mm. The double shadow in the profile of the profile of a model cannot be discerned in the interferogram when the position shift is of

the order of a micro-meter. Thus the phenomenon of the double shadow has been eliminated. At the same time, fringes with better contrast and finer details than that found in the interferograms of apparallel crystal interometer are produced. Furthermore, the reflection at the bottom surface of the prism is almost a total internal reflection, the brightness of the interferogram is much greater than that of the parallel crystal interferometer. This in particular is of advantage to the high speed photographic recording of fast processes with a much shorter exposure time. From photo 5 and 6 in picture page 14 we can make the comparison. The former is the photograph of a hot nail taken with a parallel crystal interferometer while the latter is the photograph of the same phenomenon taken with the improved apparatus. We can see that the double shadow is eliminated, and that the brightness has increased and the fringes finer. This is suitable in the measurement of such flow field as that of a supersonic wind tunnel which contains models.

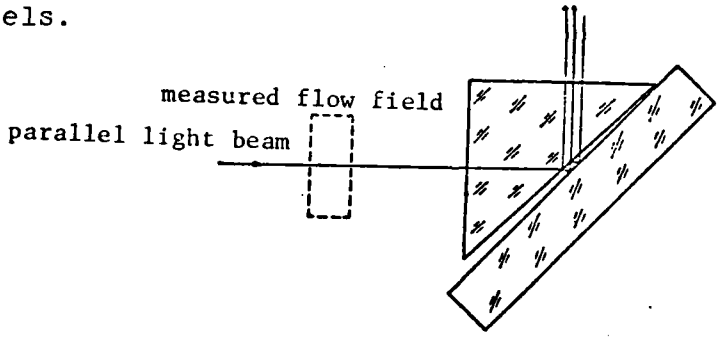

Figure 5. Air gap interference element

IV. Conclusions

The parallel crystal interferometer is better suited for measuring many types of flow fields, such as the flow fields in aerodynamics, fluid dynamics, physics of explosion, heat conduction, and laser physics; it can be adapted to adverse measuring environment and has greater practicality. It

is simpler to design and construct and is easier to be calibrated and used. It is specially good for measuring supersonic flow field. It is also good for testing the quality of optical elements.

REFERENCES

[1] Bryngdahl, O., Progress in Optics, E. Wolf, Ed., Vol. 4 (1965), 39.
[2] Kelley, J. G., *Appl. Opt.*, 9, 4 (1970), 948.
[3] Merzkirch, W., *Appl. Opt.*, 13, 2 (1974), 409.
[4] Ladenburg, R., Physical Measurements in Gas Dynamics and Combustion, Princeton University Press. (1954), 47.

RESEARCH NOTES

NUMERICAL SOLUTION OF NAVIER-STOKES EQUATIONS

Guo Benyu Shanghai University of Science and Technology
Guo Benqi Jiujiang Refinery

I. There are many methods to compute Navier-Stokes equations but few are able to prove their estimation of errors, mainly because it is difficult to treat the non-linear term and the ratio of pressure to density. Artificial state equation was used in references [3] and [4] while Guo Benyu [6] combined the method in reference [5] and proved the stability of the implicit scheme. However he has not proved the convergence of the explicit scheme nor has he been able to derive the convergence of P from this. Another method to solve the Navier-Stokes equations is to compute directly the Poison equation of P. For convenience, let us take the following two dimensional equations as an example:

$$\left.\begin{aligned} &\frac{\partial U}{\partial t}+U\frac{\partial U}{\partial x}+V\frac{\partial U}{\partial y}-\nu\nabla^2U+\frac{\partial P}{\partial x}=f_1\\ &\frac{\partial V}{\partial t}+U\frac{\partial V}{\partial x}+V\frac{\partial V}{\partial y}-\nu\nabla^2V+\frac{\partial P}{\partial y}=f_2\\ &\nabla^2P=2\frac{\partial U}{\partial x}\frac{\partial V}{\partial y}-2\frac{\partial V}{\partial x}\frac{\partial U}{\partial y}+f_3 \end{aligned}\right\} \qquad (1.1)$$

where U, V are respectively the velocity components along x, y directions is the coefficient of viscosity, f_i(i-1,2,3) are known functions. Furthermore the initial and boundary values of U, V and P are assumed known.

In this paper we extend the result in [5] and construct several schemes which are convenient for computation. We also have extended a non-linear inequality in [5], thus solving the problem of rigorous error estimation.

II. Let h, τ respectively denote the step lengths along the space and time directions of the net. $\lambda = \tau/h^2$, Q is a net point. R_h represents the collection of internal points of the net region to be solved for with Γ_h as its boundary. w(k) or w both denote w(ih,jh,kτ). $\bar{w} = \bar{w}(k) = w(k+1)$, $w_x, w_{\bar{x}}, w_{x\bar{x}}, w_t, w_{\bar{t}}, \Delta w$ all have the same meaning as in reference [5]. We further define

$$(w, u) = \sum_{Q \in R_h} h^2 w(Q) u(Q), \quad \|w\|^2 = (w, w), \quad \|w\|_1^2 = \|w_x\|^2 + \|w_y\|^2$$

$$s(w) = \sum_{Q \in R_1 + R_2} w^2(Q)$$

where R_1, R_2 are the collections of the internal points with minimum x,y coordinate values respectively.

$$s_1(w) = \|w\|_1^2 + s(w)$$

Lemma Let w(k) be a non-negative net function, g_0, L, τ, d are positive constants. $\rho(T)$ is a non-negative continuous function of T, and when $w_i \leqslant d (i \leqslant k-1)$, the functionals

$$H_w(k-1) = H[w(0), \cdots, w(k-1)] \leqslant Lw(k-1)$$
$$G_w(k) = G[w(0), \cdots, w(k)] \geqslant g_0 w(k)$$

then if

$$g_0 w(0) \leqslant \rho(T) \leqslant e^{-LT/g_0} \cdot d g_0$$

and when $1 \leqslant k \leqslant \left[\frac{T}{\tau}\right]$ 时,

$$G_w(k) \leqslant \rho(T) + \tau \sum_{i=0}^{k-1} H_w(j)$$

then

$$w(k) \leqslant \frac{\rho(T)}{g_0} e^{LT/g_0}$$

Note 1. If

$$H_w(k) = C_0\left[w(k) + \frac{w^2(k)}{h^2}\right] + \left[C_1 \frac{w(k)}{h^2} + C_2 - C_3\right] v(k)$$

$$G_w(k) = [1 - C_4\tau - w(k-1)]w(k)$$

where $v(k)$ is a non-negative net function and τ, h are sufficiently small, and there exists constant M such that $C_1M - C_2 \leqslant C_3$, then we may take

$$d = Mh^2, \quad g_0 = \frac{1}{2}, \quad L = C_0(M+1)$$

Thus when $\rho \leqslant \frac{1}{2} e^{-2C_0T(M+1)} \cdot d$ 时,

$$w(k) \leqslant 2\rho e^{2C_0T(M+1)}$$

Note 2. In Note 1, $\rho \leqslant M_0 h^2 T$, $C_1 = b_1 r$, $C_2 = b_2 r$ where b_1, b_2, C_3 are constants, r is to be determined, $C_0(r)$ is a continuous function of r, hence if $T \leqslant T_0$ for T_0 sufficiently small so that $2T_0M_0e^{4C_0T_0} \leqslant 1$, then we may take

$$r = \frac{C_3}{b_1 + b_2}, \quad L = 2C_0, \quad g_0 = \frac{1}{2}$$

Thence

$$w(k) \leqslant 2\rho e^{4C_0T}$$

III. The double scheme to solve (1.1) is

$$\left.\begin{aligned} &u_t + d(u, u, v) - \nu\Delta(u + \sigma\tau u_t) + P_x = f_1, && R_h \times S_\tau^0 \\ &v_t + d(v, u, v) - \nu\Delta(v + \sigma\tau v_t) + P_y = f_2, && R_h \times S_\tau^0 \\ &\Delta P = \phi(u, v) + f_3, && R_h \times S_\tau^0 \end{aligned}\right\} \tag{3.1}$$

where $0 \leqslant \sigma, \alpha \leqslant 1$ are non-negative parameters, S_r^0 denotes the set $E\{t \mid t = k\tau, k = 1, 2, \cdots\}$,

If
$$\phi(u, v) = (u_x^* v)_y - (\nu u_y)_x^* + (v_y^* u)_x^* - (\nu_x^* u),$$
$$d(w, u, v) = \alpha(wu)_x^* + \alpha(wv)_y + (1 - \alpha)\nu w_x^* + (1 - \alpha)\nu w$$

$$\alpha = 1/2, u|_{\Gamma_h} = v|_{\Gamma_h} = 0$$

then
$$(u, d(u, u, v)) = (v, d(v, u, v)) = 0$$

This, in practice, simulates the following conservation law and hence yields a better numerical result:

$$\iint_R \left(U\frac{\partial U}{\partial x} + V\frac{\partial U}{\partial y}\right) U dx dy = \iint_R \left(U\frac{\partial V}{\partial x} + V\frac{\partial V}{\partial y}\right) V dx dy = 0$$

Let us denote the errors by $\tilde{u}(k), \tilde{v}(k), \tilde{P}_i$, and let $\varepsilon = (\tilde{u}, \tilde{v}), \|\varepsilon\|^2 = \|\tilde{u}\|^2 + \|\tilde{v}\|^2$,

then

$$\|\varepsilon_t\|^2 = \|\tilde{u}_t\|^2 + \|\tilde{v}_t\|^2, \quad \|\varepsilon(k)\|^2_{\hat{\omega}_\tau} = \|\varepsilon(k)\|^2 + \tau\nu \sum_{j=0}^{k-1} \|\varepsilon(j)\|^2, \quad \|\varepsilon_t\|^2 = \|\tilde{u}_t\|^2 + \|\tilde{v}_t\|^2$$

Theorem I. In scheme (3.1), if (1) $\nu > 0$, (2) $\sigma \geq \frac{1}{2}$ or $\lambda < \frac{1}{9\nu(1/2-\sigma)}$, , then there exists positive number T_o and C such that when $T \leq T_o$ and

$$\rho = \|\varepsilon(0)\|^2 + \tau \sum_{j=0}^{k-1} \sum_{i=1}^{3} \|\tilde{f}_i(j)\|^2 \leq h^2 \cdot C$$

$\|\varepsilon(k)\|^2_{\hat{\omega}_\tau} \leq M\rho e^{LT}$, where L, M are positive constants related only to m_0, a, ν, σ, λ and u, v and the upper limit N of the absolute value of their first order difference quotients. If $\rho = 0(h^2)$, then T_o is arbitrary.

Proof: Obviously we have the error equations

$$\left.\begin{aligned} L_1(\tilde{u}, \tilde{v}, \tilde{p}) &= \tilde{u}_t + d(\tilde{u}, u+\tilde{u}, v+\tilde{v}) + d(u, \tilde{u}, \tilde{v}) - \nu\Delta(\tilde{u} + \sigma\tau\tilde{u}_t) + \tilde{p}_x = \tilde{f}_1 \\ L_2(\tilde{v}, \tilde{u}, \tilde{p}) &= \tilde{v}_t + d(\tilde{v}, u+\tilde{u}, v+\tilde{v}) + d(v, \tilde{u}, \tilde{v}) - \nu\Delta(\tilde{v} + \sigma\tau\tilde{v}_t) + \tilde{p}_y = \tilde{f}_2 \\ \Delta\tilde{p} &= \tilde{\psi}(\tilde{u}, \tilde{v}) + \tilde{f}_3 = \phi(\tilde{u}, \tilde{v}) + \phi(u, \tilde{v}) + \phi(\tilde{u}, v) + \tilde{f}_3 \end{aligned}\right\} \quad (3.2)$$

If we compute the quantity $(2\tilde{u} + m\tau\tilde{u}_t, L_1(\tilde{u}, \tilde{v}, \tilde{p})) + (2\tilde{v} + m\tau\tilde{v}_t, L_2(\tilde{u}, \tilde{v}, \tilde{p}))$, then similar to (5) we get

$$\|\varepsilon\|_t^2 + (m-1)\tau\|\varepsilon_t\|^2 + \nu s_1(\varepsilon) + \tau^2\nu\left(m\sigma - \frac{m}{2} - \sigma\right)s_1(\varepsilon_t)$$

$$+ \tau\nu\left(\sigma + \frac{m}{2}\right)s_1(\varepsilon)_t + (\nu - aA)\|\varepsilon\|_t^2 - aB\|\varepsilon\|^2 \leq \tilde{R}(\varepsilon)$$

where A, B, M_1 are positive numbers unrelated to h and τ and a, a_1 are positive parameters to be suitable determined.

$$\tilde{R}(\varepsilon) \leq M_0\left\{\left(1 + \frac{1}{a_1}\right)(\|\varepsilon\|^2 + \|\tilde{\varepsilon}\|^2) + \frac{1}{h^2 a}(\|\varepsilon\|^4 + \|\varepsilon\|^2\|\tilde{\varepsilon}\|^2) + \|\tilde{f}_1\|^2 + \|\tilde{f}_2\|^2\right\} + a_1\|\tilde{p}\|^2$$

Following the method in (5), we choose a and m suitable and sum the above equation in the t direction and obtain

$$\|\varepsilon(k)\|^2_{\hat{\omega}_\tau} \leq M_1\|\varepsilon(0)\|^2 + \left(\sigma + \frac{m}{2}\right)\tau s[\varepsilon(0)] + \tau \sum_{j=0}^{k-1} \tilde{R}(\varepsilon) \quad (3.3)$$

From the third equation of (3.2), we get

$$-s_1(\tilde{p}) = (\tilde{p}, \tilde{\phi}) + (\tilde{p}, \tilde{f}_3), \quad \|\tilde{p}\|_1^2 \leqslant \frac{\|\tilde{p}\|^2}{8m_0} + 2m_0\|\tilde{f}_3\|^2 + |(\tilde{p}, \tilde{\phi})|$$

where

$$m_0 = \sup_{w \in r_{h=0}} \frac{\|w\|^2}{\|w\|_1^2}$$

but

$$|(\tilde{p}, \tilde{\phi})| \leqslant \frac{\|\tilde{p}\|_1^2}{8} + 48\left\{\frac{\|\varepsilon\|^2\|\varepsilon\|_1^2}{h^2} + N^2\|\varepsilon\|_1^2 + N^2\|\varepsilon\|^2\right\}$$

thence

$$\|\tilde{p}\|_1^2 \leqslant 96\left\{\frac{\|\varepsilon\|^2\|\varepsilon\|_1^2}{h^2} + N^2\|\varepsilon\|_1^2 + N^2\|\varepsilon\|^2\right\} + 4m_0\|\tilde{f}_3\|^2$$

Substitute the above into (3.3), then

$$\frac{1}{2}\|\varepsilon(k)\|_{0\oplus\nu}^2 - M_1\tau\|\varepsilon(k)\|^2 - M_2\lambda\|\varepsilon(k)\|^2\|\varepsilon(k-1)\|^2 \leqslant M_3\rho + M_3\tau\sum_{j=0}^{k-1}(\|\varepsilon(j)\|^2$$

$$+ \|\varepsilon(j)\|^4h^{-2}) + \tau\sum_{i=0}^{k-1} M_4\left(a_1\frac{\|\varepsilon(j)\|^2\|\varepsilon(j)\|_1^2}{h^2} + a_1\|\varepsilon(j)\|_1^2 - \frac{\nu}{2}\|\varepsilon(j)\|_1^2\right)$$

Now we need only suitably choose a_1 and apply note 2 in the lemma in which

$$w = \|\varepsilon\|_{0\oplus\nu}^2, v = \|\varepsilon\|_1^2, r = a_1.$$

Thus if U, V, P are suitably smooth so that (3.1) has an aymptotic accuracy of at least O(h), then scheme (3.1) converges and

$$\|\tilde{u}\|^2 + \|\tilde{v}\|^2 = O(h^4), \quad \|\tilde{p}\|^2 = O(h^2)$$

IV. The triple scheme to solve (1.1) may be constructed as follows:

$$\left.\begin{aligned} &u_t + \theta\tau^2u_{tt} + d(u, u, v) - \nu\Delta u + p_x = f_1, && R_h \times S_\tau^0 \\ &v_t + \theta\tau^2v_{tt} + d(v, u, v) - \nu\Delta v + p_y = f_2, && R_h \times S_\tau^0 \\ &\Delta p = \phi(u, v) + f_3, && R_h \times S_\tau^0 \end{aligned}\right\} \qquad (4.1)$$

in which θ is a positive parameter.

Theorem II. In scheme (4.1) if (1)$\nu > 0$, , (2) $\tau\theta$ is constant, $0 < \tau\theta \leqslant \frac{1}{2}$, (3)$\lambda < \frac{4\tau\theta}{9\nu}$ then there exist positive constants T_0 C such that when $T \leqslant T_0$, $\rho' = \rho + \|\varepsilon(1)\|^2 \leqslant Ch^2$,

$$\|\varepsilon(k)\|^2_{\tilde{S}_\tau} + \|\varepsilon(k-1)\|^2 \leqslant M\rho' e^{LT}$$

If $\rho' = 0(h^2)$, then T_0 is arbitrary.

Proof: Let $\theta = \frac{1}{2\tau} + \frac{\theta_0}{\tau}$, , then $-1/2 < \theta_0 \leqslant 0$, . Similar to Theorem I, we have

$$\|\varepsilon\|^2_{\tilde{S}_\tau} + (m-1)\tau\|\varepsilon_t\|^2 + \nu s_1(\varepsilon) - \frac{\tau^2\nu m}{2} s_1(\varepsilon_t) + \frac{\nu m\tau}{2} s_1(\varepsilon)_t + (\nu - aA)\|\varepsilon\|^2_{\tilde{S}_\tau}$$

$$- aB\|\varepsilon\|^2_{\tilde{S}_\tau} + \tau\theta_0\|\varepsilon\|^2_{\tilde{S}_\tau} - \theta_0\tau\|\varepsilon_t\|^2 - \theta_0\tau\|\varepsilon_{\bar{t}}\|^2 + \frac{\tau^2\theta_0 m}{2}\|\varepsilon_t\|^2_{\tilde{S}_\tau} + \frac{\tau^2\theta_0 m}{2}\|\varepsilon_{\bar{t}}\|^2 \leqslant \tilde{R}(\varepsilon)$$

where $\tilde{R}(\varepsilon)$ is the same as in Theorem I. Now we take m = 2/ $2+4\theta_0-9\lambda\nu$, then after summing over t, the sums of the 2nd, 4th and 12th terms in the LHS of the above equation are non-negative. The rest of the proof is similar to that used in Theorem I but we take $w(k) = \|\varepsilon(k)\|^2_{\tilde{S}_\tau} + \|\varepsilon(k-1)\|^2$ when applying lemma.

The ADE scheme to solve (1,1) is

$$\left.\begin{aligned} &u_t + d(u,u,v) - \nu\Delta u - \frac{\nu\tau}{h} H(u) + p_x = f_1, && R_h \times S^0_\tau \\ &v_t + d(v,u,v) - \nu\Delta v - \frac{\nu\tau}{h} H(v) + p_y = f_2, && R_h \times S^0_\tau \\ &\Delta p = \phi(u,v) + f_3, && R_h \times S^0_\tau \end{aligned}\right\} \qquad (4.2)$$

where H(w) assumes the forms $-w_{\bar{x}t} - w_{\bar{y}t}$, $w_{xt} - w_{\bar{y}t}$, $-w_{\bar{x}t} + w_{yt}$, $w_{xt} + w_{yt}$, etc in accordance with a definite rule.

Theorem III. In (scheme (4.2) $\nu > 0$, $\lambda < \frac{2}{\nu}$, then Theorem I is also true.

Proof: Following Theorem I we have

$$\|\varepsilon\|^2_{\tilde{S}_\tau} + (m-1)\tau\|\varepsilon_t\|^2 + \frac{\nu\tau m}{2} s_1(\varepsilon)_t + \nu s_1(\varepsilon) + (\nu - aA)\|\varepsilon\|^2_{\tilde{S}_\tau} - aB\|\varepsilon\|^2_{\tilde{S}_\tau}$$

$$- \frac{2\nu\tau}{h}(\varepsilon, H(\varepsilon)) - \frac{\tau^2\nu m}{2} s(\varepsilon_t) \leqslant \tilde{R}(\varepsilon)$$

where R(ε) is same as before. The sum of the last two terms on the LHS is not more than $\frac{\nu}{2}\|\epsilon\|_1^2+\lambda\nu\tau\left(6+\frac{m}{2}\right)\|\epsilon_t\|^2$. Now if we take $m=\frac{2+12\lambda\nu}{2-\lambda\nu}$ then the sum of the 2nd, 7th and 8th terms on the RHS of the above equation is non-negative. The rest of the proof is the same as in Theorem I.

The splitting scheme to solve (1.1) may be constructed as follows:

$$\left.\begin{aligned}
&\frac{u^*-u}{\tau}+\frac{dx}{2}(u^*+u,u)-\frac{\nu}{2}[u^*_{xx}+u_{xx}]+\frac{p_x}{2}=f_1/2, && R_h\times S_\tau^0\\
&\frac{\bar u-u^*}{\tau}+\frac{dy}{2}(\bar u+u^*,v)-\frac{\nu}{2}[\bar u_{yy}+u^*_{yy}]+\frac{p_y}{2}=f_1/2, && R_h\times S_\tau^0\\
&\frac{v^*-v}{\tau}+\frac{dx}{2}(v^*+v,u)-\frac{\nu}{2}[v^*_{xx}+v_{xx}]+\frac{p_x}{2}=f_2/2, && R_h\times S_\tau^0\\
&\frac{\bar v-v^*}{\tau}+\frac{dy}{2}(\bar v+v^*,v)-\frac{\nu}{2}[\bar v_{yy}+v^*_{yy}]+\frac{p_y}{2}=f_2/2, && R_h\times S_\tau^0\\
&\Delta p=\phi(u,v)+f_3, && R_h\times S_\tau^0
\end{aligned}\right\} \tag{4.3}$$

where

$$dx(w,u)=\alpha(wu)_x+(1-\alpha)uw_x$$
$$dy(w,v)=\alpha(wv)_y+(1-\alpha)vw_y$$

If $$\alpha=\frac{1}{2},\quad w|_{\Gamma_h}=0$$

then $$(w,dx(w,u))=(w,dy(w,v))=0$$

Hence the conservation law is simulated. If we only need to compute the P value at some moment, then the method to calculate vorticity and flow function in reference [5] may be used. Then P may be found from the following equation

$$\nabla^2 P=2\left(\frac{\partial^2\psi}{\partial x^2}\right)\left(\frac{\partial^2\psi}{\partial y^2}\right)-2\left(\frac{\partial^2\psi}{\partial x\partial y}\right)^2+f_3$$

Similar results for 3 dimensional problems may be established. Further results may be seen in (6) and (7). In this paper the generalised stability index of the corresponding 2 dimensional scheme in reference [6] is improved to $s \leq 1$. If the reverse wind method in (6) is used to compute (1.1), the scheme is also convergent.

REFERENCES

[1] Ames, W. F., *SIAM Rev.*, **15** (1973), 524—552.

[2] Roache, P. J., Computational Fluid Dynamics, Hermosa Publishers (1972).

[3] Lions, J. L., *SIAM AMS Proc.*, **2** (1970), 11—23.

[4] Chorin. A. J., *J. Comp. Phys.*, **2** (1967), 12—26.

[5] Guo Benyu (Acta Mathematica Sinica) Journal of Mathematics, 17 (1974) 242-258

[6] Guo Benyu (Scientia Sinica) Journal of Science 21 (1976), 127-131.

[7] Kuo Pen-yu (郭本瑜), *Scientia Sinica* (1977), 267—304.


DATE:
TIME